One-pot synthesis of Mg-Al layered double hydroxide (LDH) using MgO and Metakaolin (MK) as precursors

Jun Zhu [a], Bin Zeng [a], Liwu Mo [a,b,*], Fei Jin [c], Min Deng [a,b], Qingtao Zhang[d]

[a] *College of Materials Science and Engineering, Nanjing Tech University, Nanjing, Jiangsu 211800, PR China*

[b] *State Key Laboratory of Materials-Oriented Chemical Engineering, Nanjing, Jiangsu 211800, PR China*

[c] *School of Engineering, Cardiff University, CF24 3AA, UK*

[d] *Henan Xiaowei Environment Technology Co. Xinxiang city, Henan, PR China.*

* Corresponding author at: State Key Laboratory of Materials-Oriented Chemical Engineering, College of Materials Science and Engineering, Nanjing Tech University, Nanjing, Jiangsu 211800, PR China.

E-mail address: andymoliwu@njtech.edu.cn (L. Mo).

Highlights

- For the first time, MK was successfully used as the Al source to synthesize Mg-Al LDH.
- Effects of liquid/solid ratio, temperature & alkali concentration on the formation of LDH were delineated.
- The role of reactive MgO was elucidated in the one-pot synthesis of LDH.
- Zeolites may form depending on the Si/Al ratio of the solution which is governed

by the various synthesis parameters.

Keywords

- Mg-Al layered double hydroxide
- Metakaolin
- MgO
- One-pot synthesis
- Reaction mechanism

Abstract

Layered double hydroxides (LDH) are a class of basic inorganic layered compounds, which are widely used in the fields of adsorption and catalysis owing to their unique structure and properties. In previous studies, costly soluble Al salts or $Al(OH)_3$ were used as the Al sources for the synthesis of Mg-Al LDH. The present work proposes a facile and one-pot method to synthesize Mg-Al LDH in a water bath with MgO and MK as precursors, which are both obtained from abundant natural resources. The effects of liquid/solid ratio (30:1 or 60:1), synthesis temperature (55-90℃) and alkali concentration (3 or 6 mol/L) were investigated on the composition and characteristics of the synthetic products. The obtained samples were characterized by X-ray diffraction (XRD), Fourier transform infrared spectroscopy (FT-IR), Thermogravimetric analysis (TGA), Scanning electron microscope (SEM) and Nuclear magnetic resonance (NMR). Findings showed that a highly alkaline solution (6 M NaOH) promoted the dissolution

of MK, resulting in the release of trivalent Al for the formation of LDH. Increasing temperature also led to faster dissolution of MK and released more Al and Si, which resulted in the formation of both LDH and zeolite. More importantly, it was found that Mg^{2+} released during the hydrolysis of MgO combined with Al-containing substances directly to precipitate LDH, whereas its hydration product, i.e., brucite, remained stable in the alkaline condition and released little Mg^{2+} to participate in the formation of LDH. Zeolites may form depending on the Si/Al ratio of the solution which is governed by the various synthesis parameters. The findings not only shed lights on the reaction mechanism between the MgO and MK and the role of key synthetic conditions in the formation of LDH and zeolitic phases, but also demonstrated the feasibility of using widely-available, low-cost natural minerals to produce commercial adsorbents/catalysts.

1. Introduction：

Layered double hydroxide (LDH), also known as hydrotalcite-like compound (HT) or anionic clay, is a general term for a large class of natural and synthetic layered materials. The general formula of LDH can be expressed as $\left[M^{2+}_{1-X}M^{3+}_{X}(OH)_2\right]^{X+}\left(A^{n-}\right)_{x/n}\bullet H_2O$, where M^{2+} and M^{3+} are divalent and trivalent cations, respectively, X is the ratio of $\left[M^{3+}\right]/\left(\left[M^{2+}\right]+\left[M^{3+}\right]\right)$, and A is the interlayer anion of valence n (Halajnia et al., 2012; Ram Reddy et al., 2006). A wide variety of M^{2+}, M^{3+}, X, and A^{n-} produces a large class of iso-structural materials with various physical and chemical properties and wide-ranging applications. In recent decades, they have been studied extensively as

adsorbents (Daud et al., 2019; Lei et al., 2017; Liang et al., 2013), catalysts (Fan et al., 2014; Fan et al., 2016; Gunjakar et al., 2011; Mao et al., 2017), anion exchangers (Chubar et al., 2017; Goh et al., 2008; Halajnia et al., 2013), flame retardants (Gao et al., 2014; Nyambo et al., 2008), and drug delivery carriers (Ay et al., 2009; Ladewig et al., 2009). Specifically as an adsorbent, LDH has a huge potential in soil and water remediation (Siebecker et al., 2018; Zubair et al., 2017) due to its highly adjustable composition and structure, high stability, non-toxicity and excellent anion exchange capacity (Del Hoyo, 2007; Sajid and Basheer, 2016). In addition, LDH functionalized by intercalation, surface modification and other methods exhibits high selectivity and stability and hence can more effectively adsorb heavy metal ions (Gu et al., 2015; Tran et al., 2018; Zhen et al., 2020).

LDH can be prepared by co-precipitation (Miyata, 1975; Panda et al., 2011; Zhang et al., 2006), hydrothermal (Huang et al., 2015; Xu and Lu, 2005), mechanochemical (Ferencz et al., 2015; Qu et al., 2016) and sol-gel methods (Jitianu et al., 2013; Lopez et al., 1996), among which co-precipitation was most commonly used (Chubar et al., 2017) due to its easy operational procedure and the high purity of synthesized LDH. The co-precipitation of Mg-Al LDH could be considered as a simultaneous precipitation of $Al(OH)_3$ and $Mg(OH)_2$ (Theiss et al., 2016) using soluble metal salts, such as $Mg(NO_3)_2$, $AlCl_3$ as precursors (Bukhtiyarova, 2019). $NaHCO_3$ or NH_4HCO_3 was frequently used to regulate the pH as they also acted as the $(CO_3)^{2-}$ source(Ogawa and Kaiho, 2002; Zeng et al., 2009). The use of pure chemicals was not only costly, difficult to handle and transport but also unsustainable and hence various naturally-

abundant Mg and Al sources were explored. For Mg sources, dolomite (Hosni and Srasra, 2009, 2010; Kameda et al., 2007) and magnesite (Wang et al., 2013) were used, whereas for Al, Al_2O_3 (Xu and Lu, 2005), $Al(OH)_3$ (Salomão et al., 2011), red mud (Hu et al., 2017) and ground granulated blast furnace slag (Yi et al., 2016) were attempted. However, the low reactivities of these precursors usually necessitates various pretreatments or activation processes such as acid leaching, grinding, hydrothermal treatment in order to enhance the reaction kinetics (Mao et al., 2018; Qu et al., 2016). On the other hand, reactive MgO, which can be calcined from magnesite, dolomite or synthesized from Mg-containing brines, has been successfully used as a low-cost and sustainable precursor in the synthesis of LDHs with different interlayer anions(Salomão et al., 2011; Xu and Lu, 2005). The low calcination temperature leads to smaller crystallite size, higher surface energy and hence faster dissolution rate of reactive MgO in aqueous solutions (Mejias et al., 1999; Mo et al., 2010), which facilitates the formation of LDH via the co-precipitation method.

Kaolin is a common industrial material used in paper and ceramics production rich in kaolinite ($Al_2Si_2O_5(OH)_4$), of which the world production reached 42 million tons in 2019 (2020). Upon heating at approximately 600-900℃, metakaolin (MK) is produced with enhanced chemical reactivity via the dehydroxylation of kaolinite , and hence it is commonly used as a pozzolanic material in cement and concrete (Rashad, 2013; Zhuang et al., 2016). Commercial MK typically contains 50-55% SiO_2 and 40-45% Al_2O_3 in its composition (Poon et al., 2001). Under alkaline conditions, MK readily dissolves to release $[SiO_2(OH)_2]^{2-}$, $[SiO(OH)_3]^-$ and $[Al(OH)_4]^-$. The silicate unit then condenses

106 with $[Al(OH)_4]^-$ to produce aluminosilicates (Weng and Sagoe-Crentsil, 2007), which
107 has been widely explored to manufacture geopolymers (Zhang et al., 2016). However,
108 to the best of authors' knowledge, MK has never been studied as an Al source to
109 synthesize Mg-Al LDH. Considering the wide availability and abundance of clays in
110 the world, utilization of MK would promote the concept of green chemistry and
111 potentially reduce the cost of LDH notably.
112 This article explores the feasibility of using solid MgO and MK as precursors to
113 synthesize Mg-Al LDH. The effects of alkali concentration, temperature and
114 liquid/solid ratio on the synthesized products were investigated, and the reaction
115 mechanism between MgO and MK was explored with a variety of techniques such as
116 X-ray diffraction (XRD), thermogravimetric analysis (TGA), Scanning Electron
117 Microscopy (SEM) and Nuclear Magnetic Resonance (NMR). This work would help
118 pave the way forward to future upscaling the production of low-cost high-performance
119 LDH/zeolite-based adsorbents/catalysts in a wide variety of applications.

120 **2. Materials and methods**

121 2.1. Materials

122 Highly reactive MgO (obtained from Baymag, Canada) was used, which contained a
123 small amount of dolomite and calcite as impurities (Fig. 1a). The activity value was
124 determined to be 45 seconds (denoted as M45) according to the method described in
125 the literature (Mo et al., 2010). MK, mainly in the form of amorphous aluminosilicate
126 (Mo et al., 2018)(Fig. 1b), was provided by SUPER Kaolin Co., Ltd., Inner Mongolia,

China. X-ray fluorescence (XRF) test showed that MK contained 41.08% Al_2O_3 and 52.77% SiO_2 while the purity of MgO is 91.79%. Analytical reagent grade granular NaOH and powdered Na_2CO_3 used in this study were obtained from China Xilong company. Deionized water was used throughout the study.

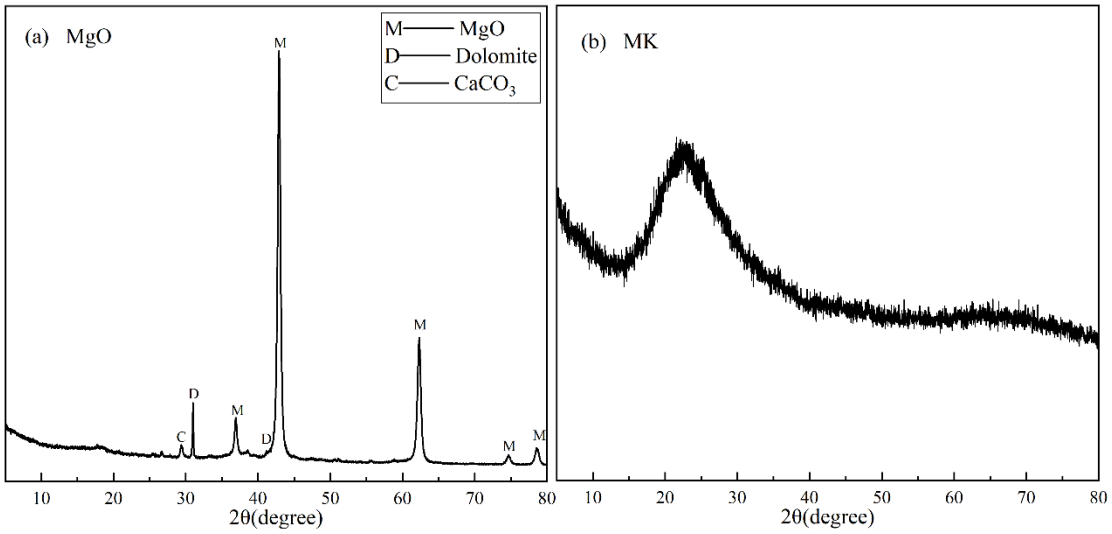

Fig. 1. XRD patterns of the raw materials (a) MgO (PDF#79-0612) Dolomite(PDF#84-1208) $CaCO_3$(PDF#72-1214) and (b) Metakaolin(MK).

2.2. Synthesis of Mg-Al LDH

In total seven (7) mixtures were prepared aiming to investigate the effects of liquid/solid ratio, alkali (NaOH) concentration, synthesis temperature and presence of Na_2CO_3 on the synthesized product. Compositions of all mixtures are detailed in Table 1. For example, MMS-1 (6:1:2-30L-6M-80℃) was made from 4.81g MK and 5.19g MgO with a Mg/Al molar ratio of ~3 in an aqueous suspension. The solid MgO and MK powders were added to a 300 mL solution containing 4.59 g 3.79g anhydrous Na_2CO_3 and 72 g NaOH (6M NaOH solution). The liquid/solid ratio was 30:1, which referred to the ratio

142 of the volume of the solution to the mass of MgO and MK. The synthesis was carried
143 out in sealed beakers, heated in a water bath and stirred at 300 rpm at the set temperature.
144 After 24 hours, the samples were filtered and washed until the pH value of filtrate
145 stabilized. Then they were dried in the oven at 80℃ for approximately 6 hours and
146 gently milled to powders. All the dried samples were bagged and stored in a desiccator.
147 Moreover, the effect of reaction time was studied for samples MMS-1 and MMS-4.
148 Table 1 Mix proportion and experimental conditions for the synthesis of LDH

Sample ID	Molar ratio	Liquid to Solid ratio	NaOH concentration (mol/L)	Temperature (℃)
MMS-1 (6:1:2-30L-6M-80℃)	MgO:MK:Na_2CO_3=6:1:2*	30:1	6	80
MMS-2 (6:1:2-30L-3M-80℃)	MgO:MK:Na_2CO_3=6:1:2	30:1	3	80
MMS-3 (6:1:2-60L-6M-80℃)	MgO:MK:Na_2CO_3=6:1:2	60:1	6	80
MMS-4 (6:1:2-30L-6M-55℃)	MgO:MK:Na_2CO_3=6:1:2	30:1	6	55
MMS-5 (6:1:2-30L-6M-90℃)	MgO:MK:Na_2CO_3=6:1:2	30:1	6	90
MMS-6 (2:1:2-30L-6M-80℃)	MgO:MK:Na_2CO_3=2:1:2	30:1	6	80
MM (6:1 -30L-6M-80℃)	MgO:MK =6:1	30:1	6	80

149 * Since 1 mol MK contains approximately 2 mol Al, this molar ratio is equivalent to
150 Mg:Al:CO_3^{2-} =3:1:1

151 2.3. Characterization

152 2.3.1. XRD

153 The synthesized products were sieved to <80 μm and then subjected to powder XRD.

The instrument used was a Rigaku SmartLab X-ray diffractometer (Cu target, rated power 3 kW, scanning range of 5°-80° with a step size 0.02° and scanning speed of 10°/min.

2.3.2. Fourier transformed infrared spectroscopy (FTIR)

The FTIR spectra of solid products were recorded on the Nexus 670 Spectrometer. Specifically 1 mg sample and 200 mg KBr in a dry environment was fully ground into a tablet, and the spectrum was measured with a resolution of 2 cm^{-1} in the wavenumber range of 4000-400 cm^{-1}.

2.3.3. Thermogravimetry/differential scanning calorimetry (TG/DSC)

The TG/DSC test used a Netzsch STA 449 differential thermogravimetric analyzer. Approximately 10 mg sample was heated from 30 to 900°C at a rate of 10°C/min in N_2 atmosphere.

2.3.4. Scanning Electron Microscopy/Energy-dispersive Spectroscopy (SEM/EDS)

The morphology of the products after gold sputtering was observed with Zeiss Ultra55 Field Emission-SEM (FE-SEM), while the elemental composition was measured by Energy Dispersive Spectroscopy (EDS).

2.3.5. Specific surface area and pore size analysis.

The pore size distribution and BET specific surface area of samples were measured by N_2 adsorption using Micro-meritics ASAP 2020 volumetric instrument. All the samples

were degassed at 180 °C prior to the test.

2.3.6. NMR

The NMR spectra were collected using the Bruker AVANCE III 400 (9.8 T) spectrometer. ^{27}Al MAS NMR spectra were collected at 104.198 MHz and a spinning speed of 12 kHz, employing a pulse width of 3.75 s (25°), a relaxation delay of 2 s with a minimum of 1024 scans.^{29}Si MAS NMR spectra were collected at 79.435 MHz at a spinning speed of 6.8 kHz and employed a pulse duration of 4.7 μs (90°) and a relaxation delay of 1.0-5.0 s, with a minimum of 1200 scans.

3. Results

3.1. XRD

As shown in Fig. 2, the characteristic diffraction peaks of Mg-Al LDH (PDF #89-0460) are observed in all samples. The reflections of (012), (015) and (018) are particularly strong, which is consistent with the characteristics of the 3R1 polytype hydrotalcite (Newman et al., 2002; Xu and Lu, 2005) due to the low synthesis temperature employed in this study. The crystal transition temperature of 110℃ was reported for the 3R2 polytype (Budhysutanto et al., 2010). Characteristic peaks for brucite ($Mg(OH)_2$, PDF #75-1527) are also prevalent in the solid products. According to (Xu and Lu, 2005), $Mg(OH)_2$ may either be an unreacted mesophase in the synthesis of LDH or an accompanying impurity, which will be elucidated in the Discussion section.

Comparing the relative intensities of LDH in each sample, it can be deduced that either

high liquid/solid ratio (MMS-3) or low synthesis temperature (MMS-4) facilitates the formation of Mg-Al LDH as the main impurities are brucite and unreacted MgO. On the other hand, sodalite and zeolite phases are generated in other samples, indicating that part of Al released from MK does not participate in the formation of Mg-Al LDH but react with Na and Si instead. Specifically, decrease of alkali concentration (MMS-1 vs. MMS-2), decrease of Mg/Al ratio in the precursors (MMS-1 vs. MMS-6), changing the reaction temperature (MMS-4 vs. MMS-1 vs MMS-5) and lack of Na_2CO_3 (MMS-1 vs. MM) all lead to the reduction of peak intensities ascribed to Mg-Al LDH in the final products. Moreover, lower alkali concentration (MMS-2) and lack of Na_2CO_3 (MM) result in the formation of Zeolite A (PDF #38-0241) and Zeolite 21 (PDF#27-1405), respectively apart from sodalite (PDF#76-1639).

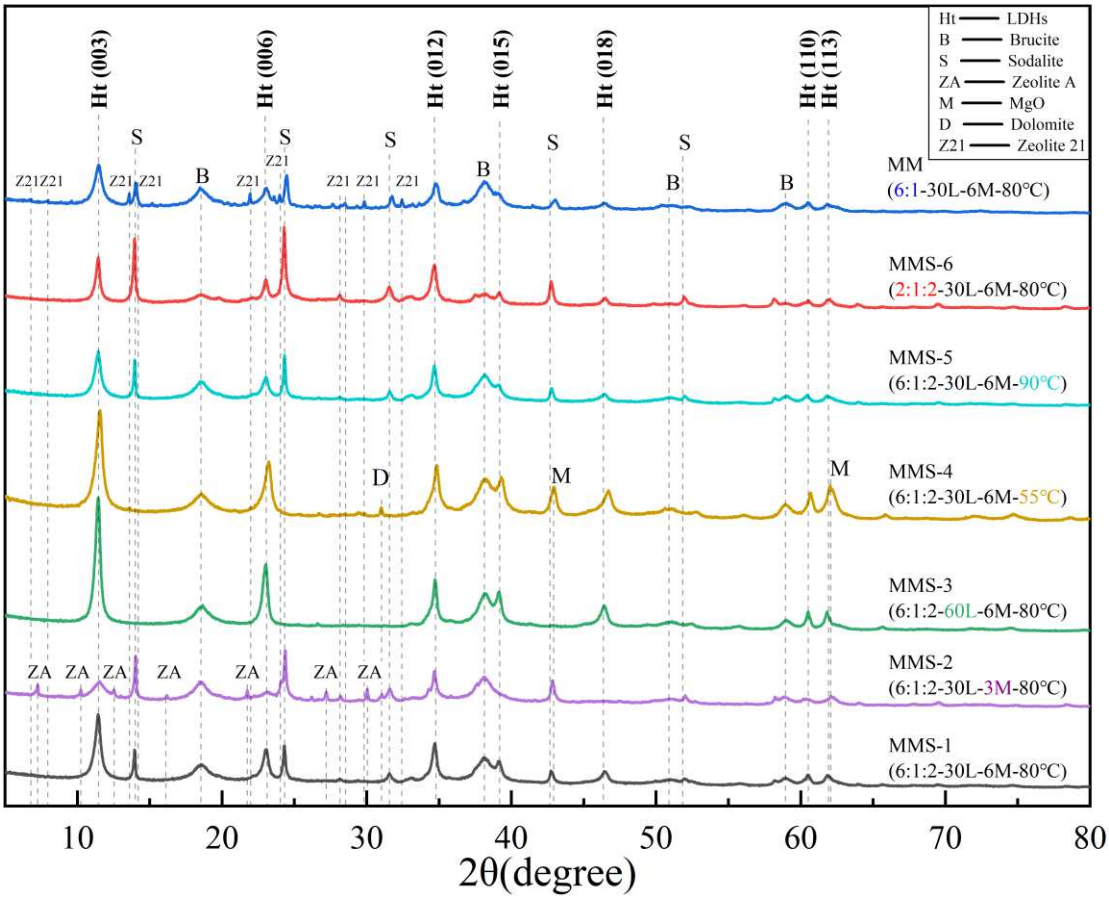

Fig. 2. XRD patterns of solid products synthesized from MgO and MK after 24h of reaction.

Fig. 3 shows the effect of reaction time on the phases of the synthesized products from mixtures MMS-1 and MMS-4. It is apparent that LDH appears very early (within 30 mins) upon reaction (Fig. 3a). With time, MgO peaks decline while those of LDH intensify. Zeolite 21 starts to form at 3 hours and peaks at 4 hours before completely disappears after 18 hours, accompanied by gradually intensified peaks of sodalite. As shown in Fig. 3b, when reaction time increased from 24 to 72 hours at 55°C, zeolitic phases are observed in MMS-4, together with reduced peak intensities from MgO. Therefore it is concluded that lowering reaction temperature merely changes the kinetics without affecting the reaction products. Lower temperature leads to a slower

dissolution rate of MK and hence less Al available in the solution, being totally incorporated in LDH. Increasing the temperature and/or reaction time release more Al and Si which react to form zeolitic phases and sodalite.

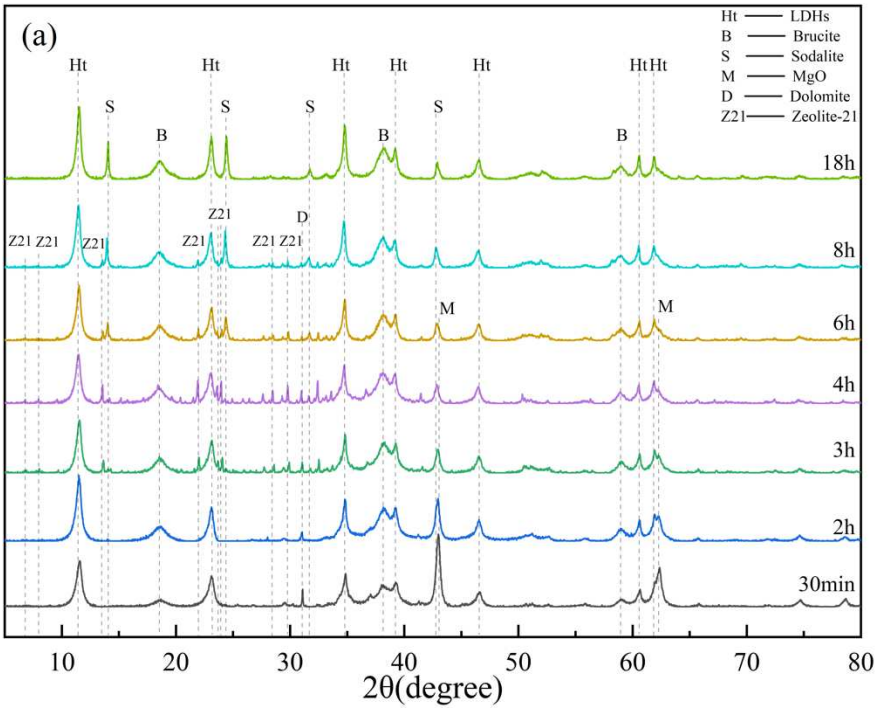

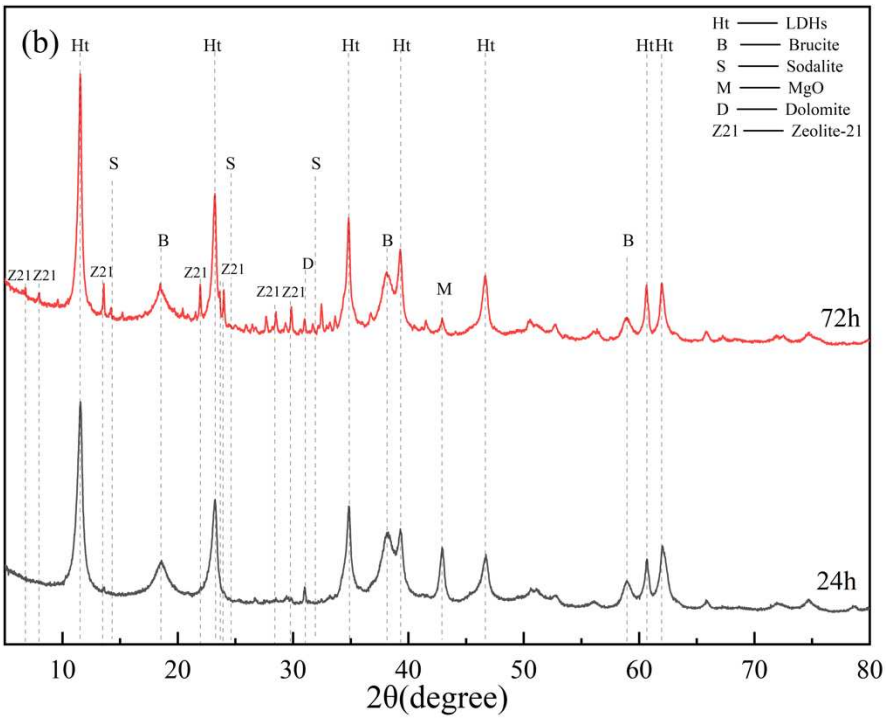

Fig. 3. XRD patterns of solid products after different reaction times (a)MMS-1 (6:1:2-30L-6M-80℃), (b)MMS-4(6:1:2-30L-6M-55℃).

3.2. FTIR

Fig. 4 shows the FTIR spectra of the solid products. The impurity phase brucite is reflected in the vibration band at 3697-3698cm^{-1}(Xu and Lu, 2005). There is a very strong broad bands in the range 3450-3530cm^{-1} due to the stretching mode of structural -OH groups in the metal hydroxide layer (Hosni and Srasra, 2009). The weak band at 1640 cm^{-1} is due to the deformation vibration of the interlayer water molecules (Mao et al., 2018). Two bands at 2362 and 1370 cm^{-1} are both ascribed to the interlayer carbonates (Guzmán-Vargas et al., 2015; Zhou et al., 2011). It is worth noting that sample MM also shows the characteristic peak of carbonate, which is due to that ambient CO_2 dissolved into the water to form carbonate, and eventually remains in the solid phase as an interlayer anion (Olanrewaju et al., 2000; Rezvani et al., 2014). The broad bands in the region of 900-1030 cm^{-1} are attributed to asymmetric Al–O/Si–O stretching vibrations (Liu et al., 2016; Rożek et al., 2018) mainly due to the presence of zeolitic phases. Two samples, i.e., MMS-3 and MMS-4, without sodalite (see Fig. 2) show no such bands. The complex bands in the range of 400-900 cm^{-1} can be assigned to hydroxyl M-OH and MO transition patterns and the specific positions depend on the nature of M^{2+} or M^{3+} ions (Mao et al., 2018).

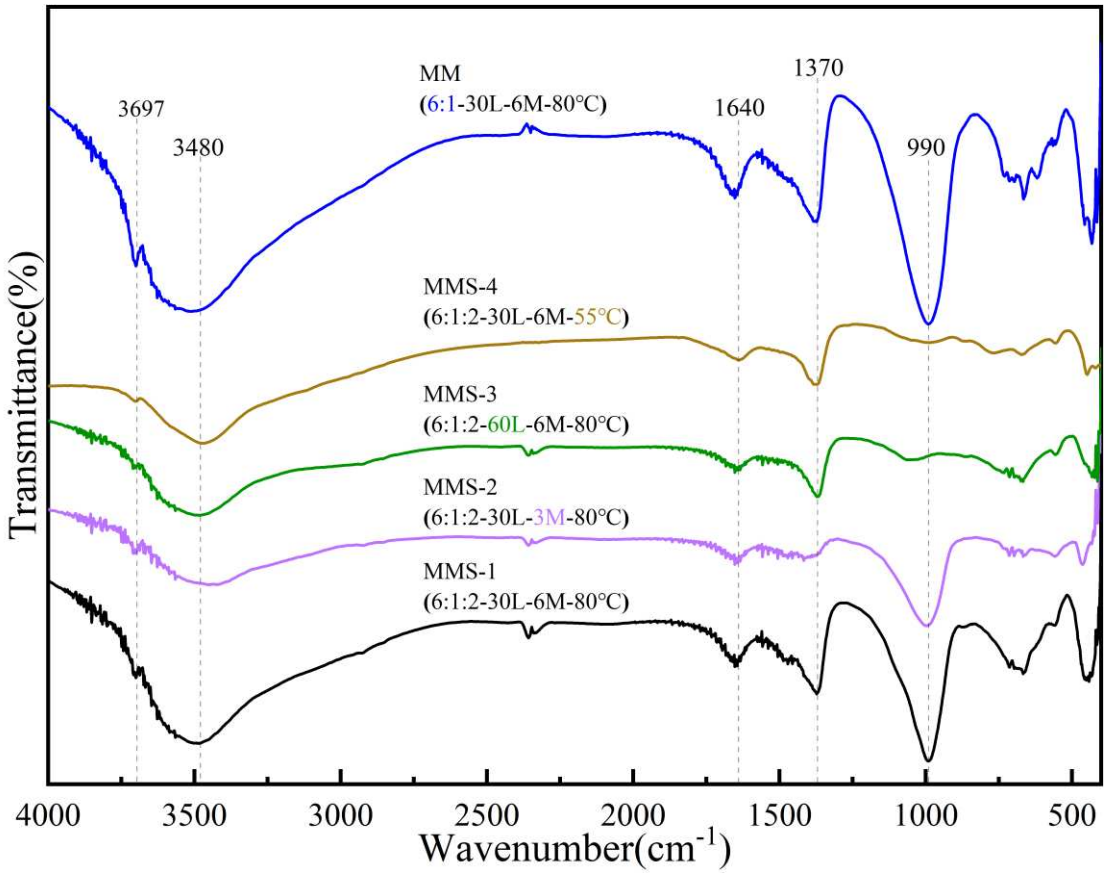

Fig. 4. FTIR spectra of solid products synthesized from MgO and MK.

3.3. Thermal analysis (TG/DSC)

Thermal analysis of the samples shows two major endothermic peaks characteristic of LDH, and two corresponding weight loss stages (Fig. 5). The first stage of weight loss starts from room temperature up to 275°C, which is mainly caused by the loss of absorbed water and interlayer water from LDH(Mao et al., 2018; Stanimirova et al., 2006). The endothermic peak of the second stage (from 275°C to 500°C) is at 430°C, which is mainly due to the decarbonisation and dehydroxylation of LDH (Bukhtiyarova, 2019; Tongamp et al., 2007). It should be noted that brucite also decomposes in this second stage (Mo et al., 2019), so it is impossible to perform a quantitative analysis by TG. The endothermic peak at 685°C is mainly due to the decomposition of the

impurities (i.e., calcite/dolomite) in the raw material.

Although accurate quantification cannot be carried out, combined with the XRD results, it can be seen that the relative intensity of the strongest LDH diffraction peak (see Fig. 2) agrees well with the mass loss of each sample. Samples MMS-3 and MMS-4 exhibit the largest mass losses due to the larger quantities of LDH formed. Samples MMS-2 and MMS-6 show the smallest mass losses which corroborates with the observation that lower alkali concentration and Mg/Al ratio reduce the amount of LDH formed. Moreover, it is deduced that the higher mass loss of MMS-2 than that of MMS-6 is mainly due to its higher brucite content (Fig. 2).

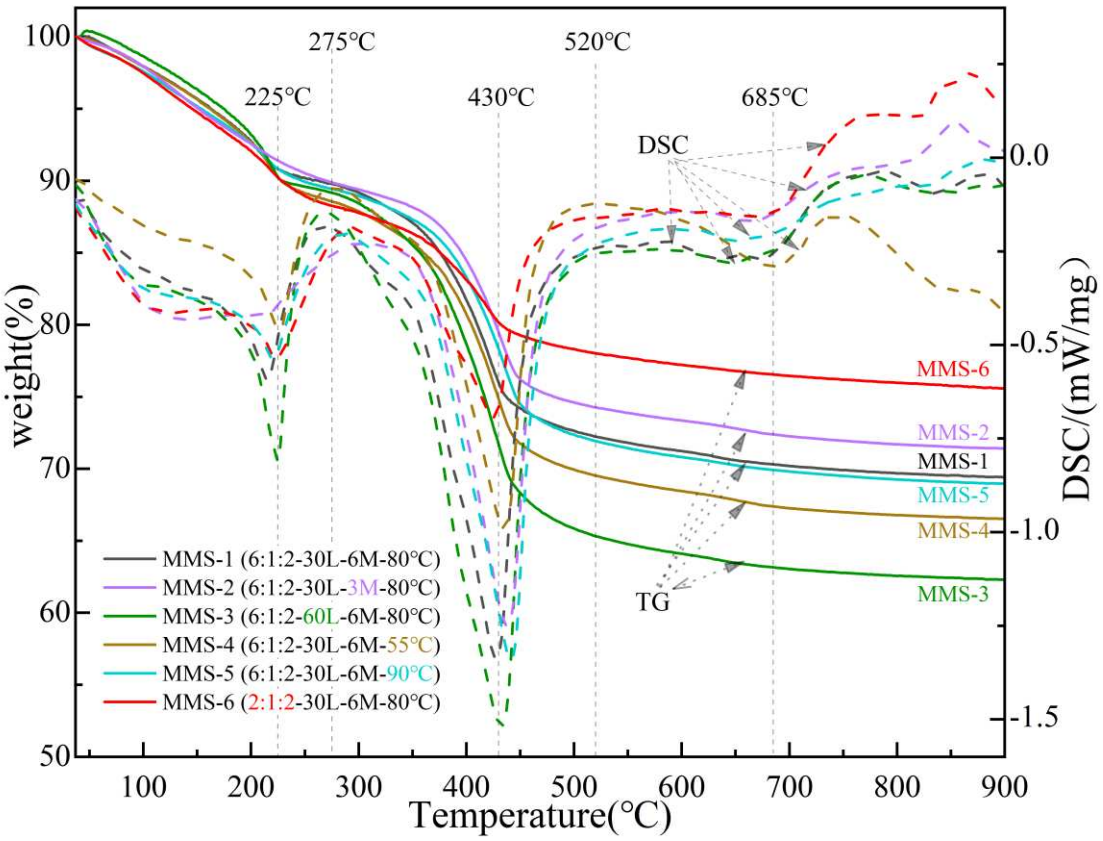

Fig. 5. TG/DSC curves of solid products synthesized from MgO and MK.

3.4. Specific surface area and pore size analysis.

From the BET results in Fig. 6a, it can be seen that the adsorption/desorption isotherm belongs to Type IV according to the IUPAC classification, with loops appearing in the high relative pressure region, corresponding to mesoporous solids (Alothman, 2012), which is typical for LDHs (Wang et al., 2019). The hysteresis is characterized as Type H3, indicating the solid pore shape is mainly plate-shaped slit pores (or sharp particles like cubes), with no uniform size which is common for zeolites (Leofanti et al., 1998). Fig. 6b shows the BJH results of the pore size distribution, demonstrating the wide range of pore sizes of 2-30 nm, which is due to the mixture of LDH, sodalite, zeolites and other impurities in those samples. The specific surface areas in the descending order of MMS-3, MMS-1, MMS-2, MM are 31.95 m^2g^{-1}, 24.51 m^2g^{-1}, 14.24 m^2g^{-1}, 12.52 m^2g^{-1}, respectively. This is comparable to the specific surface area value (17.2 m^2g^{-1}) of pure Mg-Al LDH measured by others (Tran et al., 2018).

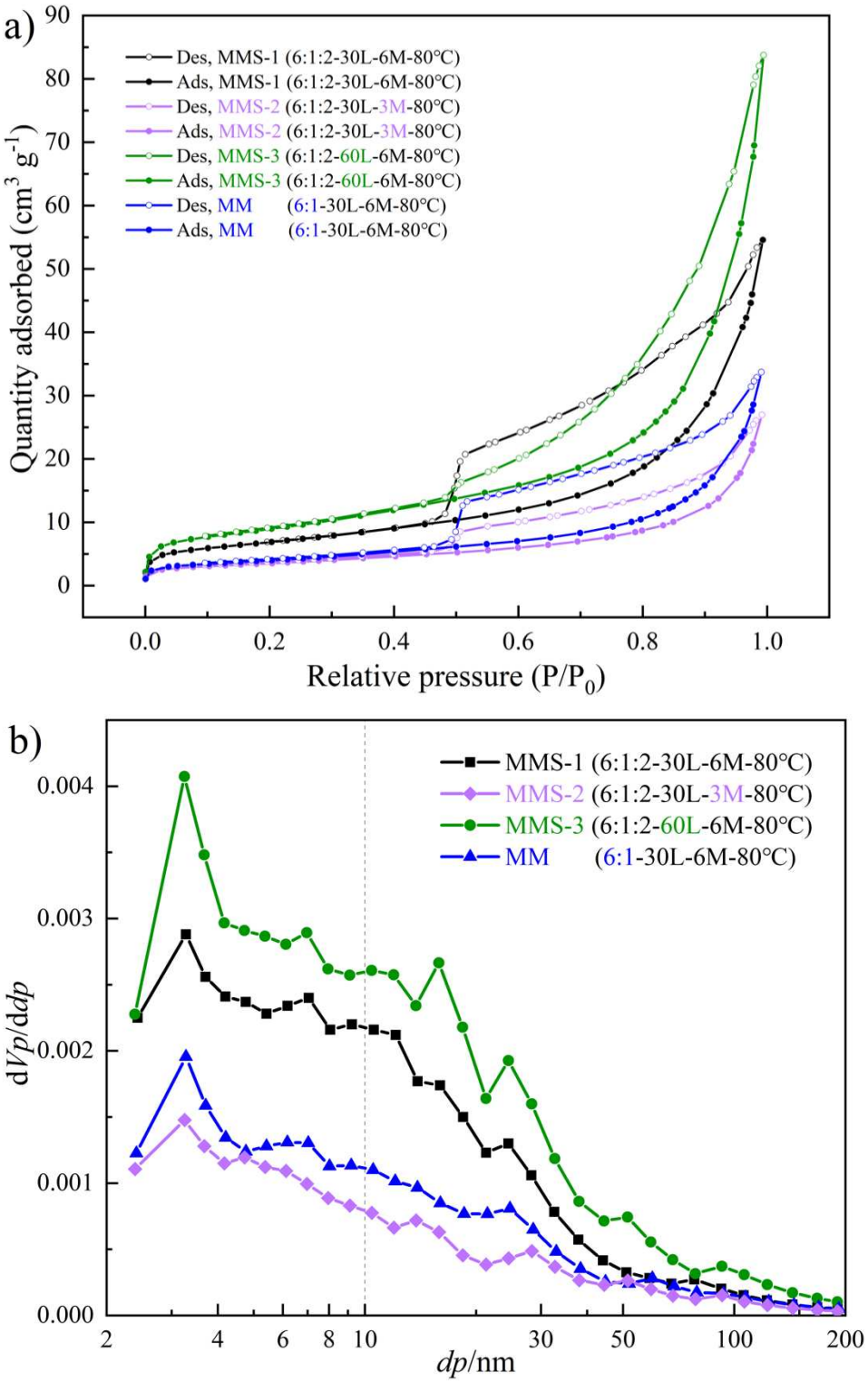

Fig. 6. BET test results of solid products synthesized from MgO and MK. (a) N_2 physisorption isotherm and (b) pore size distribution calculated by BJH method.

3.5. SEM

Fig. 7 is the scanning electron micrograph of MMS-1 sample. Fig. 7(a) shows that, unlike the regular hexagons obtained using soluble salt solutions in previous studies (Wang et al., 2014; Zeng et al., 2009), LDH crystals mainly appear as cross-stacked irregular lamellas. This is due to the preferential growth of crystals on faces with lower energy, and similar morphological feature also reflects the mechanism of hydration/dissolution/co-precipitation of the reactants (Salomão et al., 2011). The point and mapping EDS data show that the content and distribution of carbon is low and localized, which is probably due to the formation of Mg-Al-OH LDH apart from Mg-Al-CO_3 LDH. The areas where Na, Si and Al are highly overlapped in the circle of Fig. 7(a) are ascribed to sodalite, which grows together with LDH.

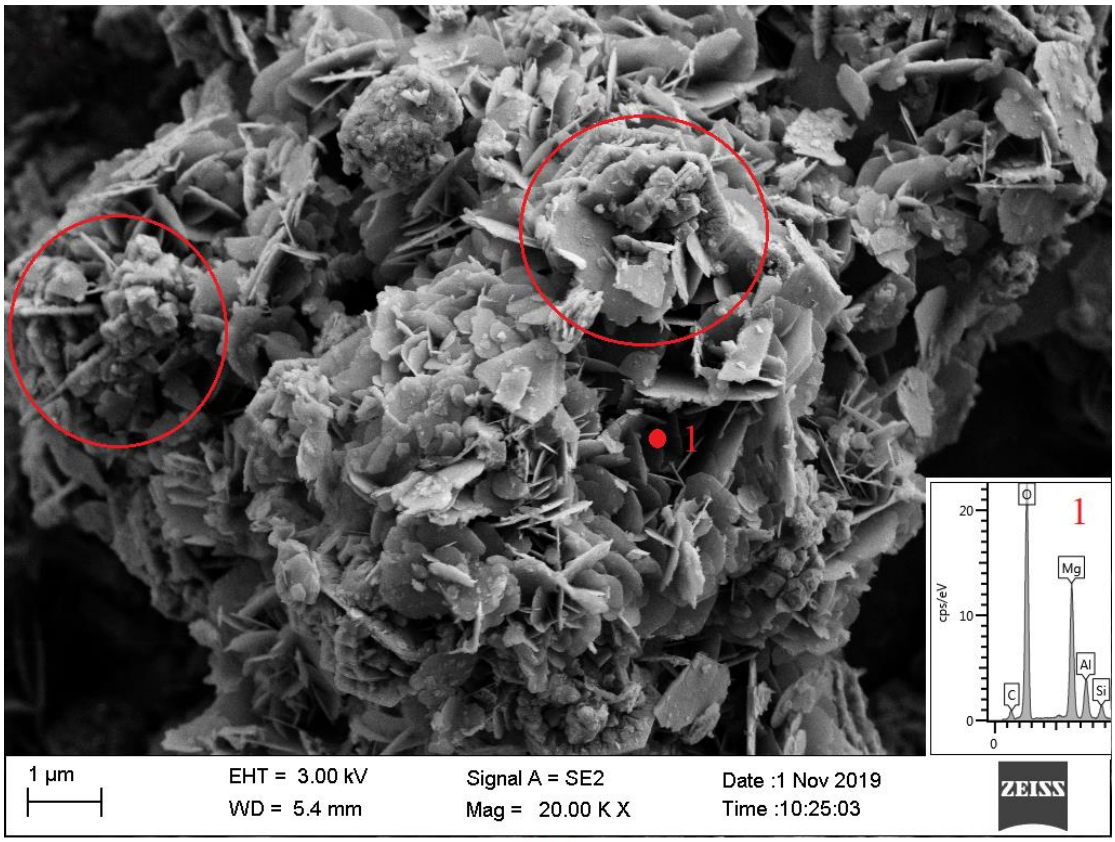

(a)

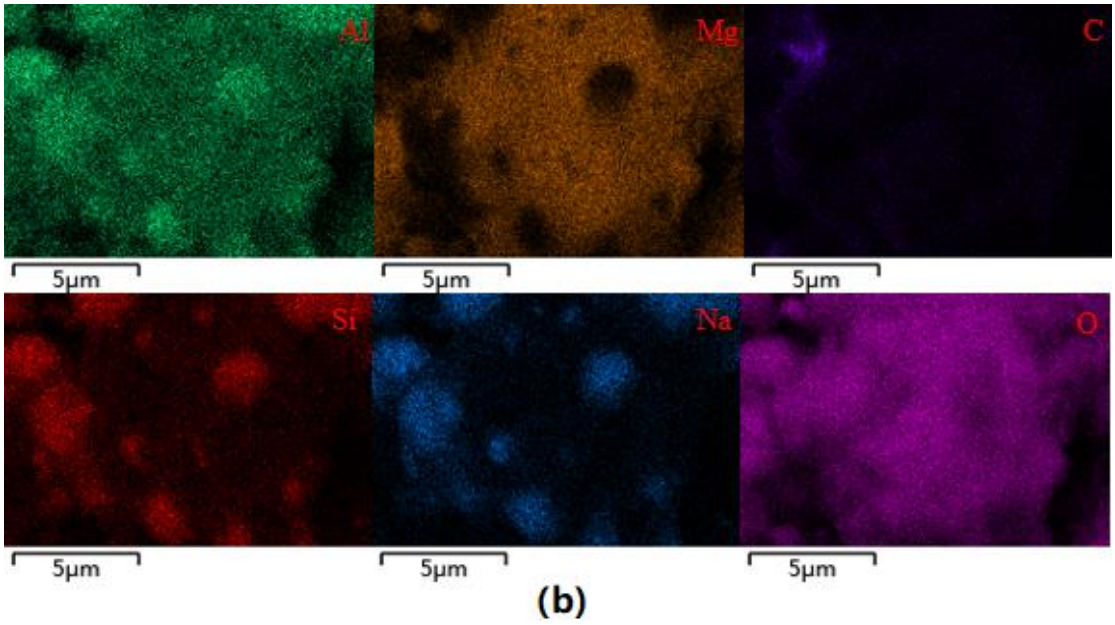

(b)

Fig. 7. (a) SEM image and EDS data at Point 1(b) EDS mapping of MMS-1 (6:1:2-30L-6M-80℃).

When the liquid/solid ratio is increased to 60:1, the sodalite diffraction peak disappears, and the morphological characteristic of the laminar LDH is much clearer (Fig. 8), which is in agreement with (Xu and Lu, 2005) where MgO is used as a magnesium source to synthesize a variety of LDHs. The sheets of Mg-Al-OH LDH are often thinner and stacked, indicating the formation of a large quantity of Mg-Al-OH LDH in the synthesized products in this work.

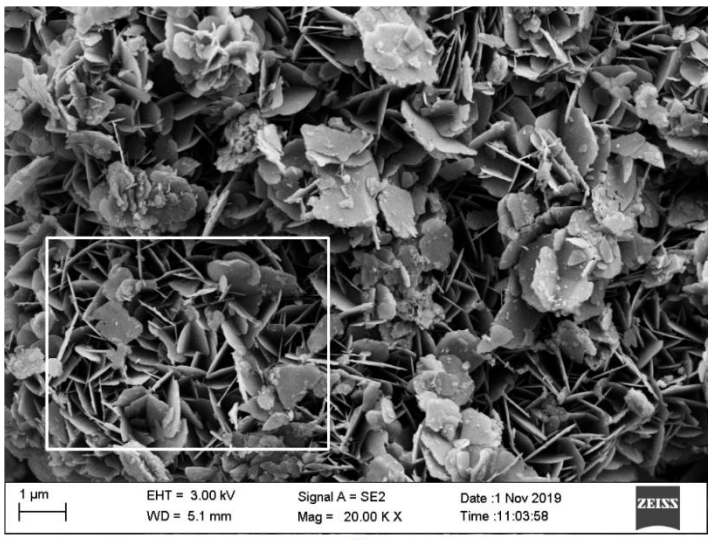

Fig. 8. SEM images of MMS-3(6:1:2-60L-6M-80°C): (a) lower magnification, (b) higher magnification on the area highlighted with a white square frame in (a).

4. Discussion

4.1. The influence of synthesis conditions

Different from the direct co-precipitation in aqueous solutions containing divalent and trivalent cations (Miyata, 1975), this study used solid MgO and MK as the Mg and Al source respectively. A strong alkaline solution (6M NaOH) was needed to break the stable silicon-oxy-aluminum bond to release the trivalent Al^{3+} (Granizo et al., 2014; Zhuang et al., 2016). Therefore, the concentration of NaOH became the key influencing factor in the MgO-MK system. When the NaOH concentration was reduced by half to 3 mol/L, the peak intensities of LDH were the lowest while those of sodalite were not significantly affected, and zeolite A appeared. This may be due to that certain zeolite structural units remain stable at different alkalinities. Lower the alkali concentration facilitated the formation of zeolite A (Rożek et al., 2019), which in turn may be transformed into sodalite(Granizo et al., 2014).

Synthesis temperature affected the dissolution kinetics and hence the reaction products significantly. MK dissolved faster at higher temperatures and released more Al and Si in the solution to participate in the reactions. The increase in the amount of these ions would lead to an increase in the nucleation rate, facilitating polycondensation and hence increasing the amount of the polymerized zeolitic phases. Therefore, it seems that setting a low reaction temperature is beneficial for LHD synthesis but on the other hand, the dissolution of MgO will be hindered, which is evidenced by the high peak intensity of MgO in sample MMS-4.

Increasing the liquid/solid ratio from 30:1 to 60:1 (Fig. 2, MMS-1 vs. MMS-3) resulted in the disappearance of the sodalite. For the formation of crystalline zeolites and sodalite, MK must undergo hydrolysis to produce sufficient Si and Al ions in the solution, which usually requires a relatively low liquid/solid ratio (Rożek et al., 2019). When reducing the Mg/Al ratio 1:1 (Fig. 2, MMS-1 vs. MMS-6) while keeping other experimental conditions unchanged, the intensities of LDH peaks reduced while those of sodalite enhanced. Assuming that under the same alkalinity, the amount of Al and Si released were similar in the two samples but reduced availability of Mg in MMS-6 promoted the formation of sodalite.

Without Na_2CO_3 (sample MM), LDH can still be formed but with much weaker intensity (Fig. 2), together with a new zeolitic phase of zeolite 21. From the FTIR and SEM/EDS results, it can be seen that Mg-Al-OH LDH was formed and CO_3^{2-} from the air or from the raw materials (calcite and dolomite) may participate in the reactions.

4.2. Mechanism of LDH synthesis

4.2.1. Role of MgO

Reactive MgO underwent continuous hydrolysis in contact with water and during the formation and development of LDH. The higher the temperature, the faster the hydrolysis progresses, and meanwhile, a small portion of $Mg(OH)_2$ precipitated and dissolved under dynamic equilibrium. The overall reaction is as follows:

$$MgO+H_2O \rightleftarrows Mg^{2+}+2OH^- \rightleftarrows Mg(OH)_2$$

The remaining $Mg(OH)_2$ may either act as the reactant to form LDH, or as an impurity

that did not participate in the reaction. In order to clarify this, MgO was replaced with fully hydrated MgO (i.e., brucite, MH) while keeping other reaction conditions unchanged (as opposed to MMS-1) and the resulting product was subjected to XRD. Fig. 9 demonstrates that a complete hydration was achieved at 23 days when reactive MgO was continuously stirred in water at 40°C. XRD result showed no trace of LDH while sodalite and zeolite 21 were the only reaction products, demonstrating that $Mg(OH)_2$ is not suitable for the synthesis of LDH under the experimental conditions in this work. The Mg^{2+} released via hydrolysis of MgO combined with Al-containing substances directly to precipitate LDH. The precipitated brucite remained stable in a strong alkaline environment (due to its low K_{sp} value), and hence could not contribute to the formation of LDH. Similar views can be found in (Paikaray et al., 2014; Yang et al., 2012), which claimed that during the synthesis of Mg-Al LDH, Mg^{2+} was incorporated into $Al(OH)_3$ or boehmite, instead of Al^{3+} entering $Mg(OH)_2$.

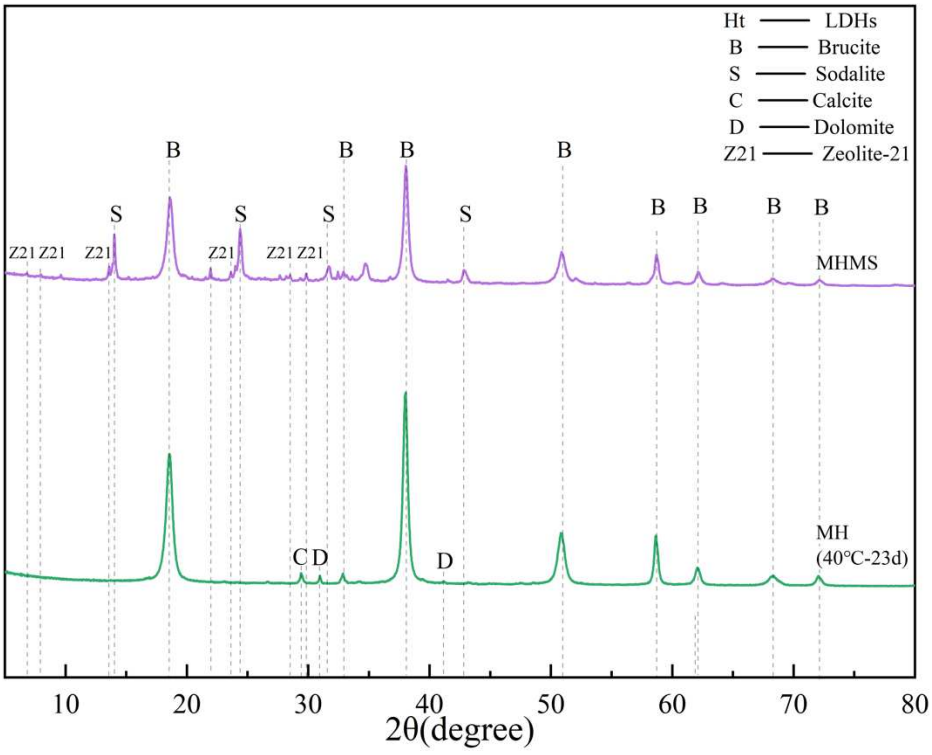

361 Fig. 9. XRD patterns of the solid product (MHMS) synthesized from hydrated MgO
362 (MH) and MK under the same conditions as MMS-1. (Hydrated
363 MgO:MK:Na_2CO_3=6:1:2, liquid/solid ratio=30:1, 6 mol/L NaOH solution, T=80℃,
364 t=24h).

365 4.2.2. Insights from ^{27}Al, ^{29}Si NMR

366 For sample MMS-3, ^{27}Al and ^{29}Si NMR were conducted on the liquid filtrate and solid
367 product and compared with those in the original MK in order to reveal the evolution of
368 Al and Si during synthesis.

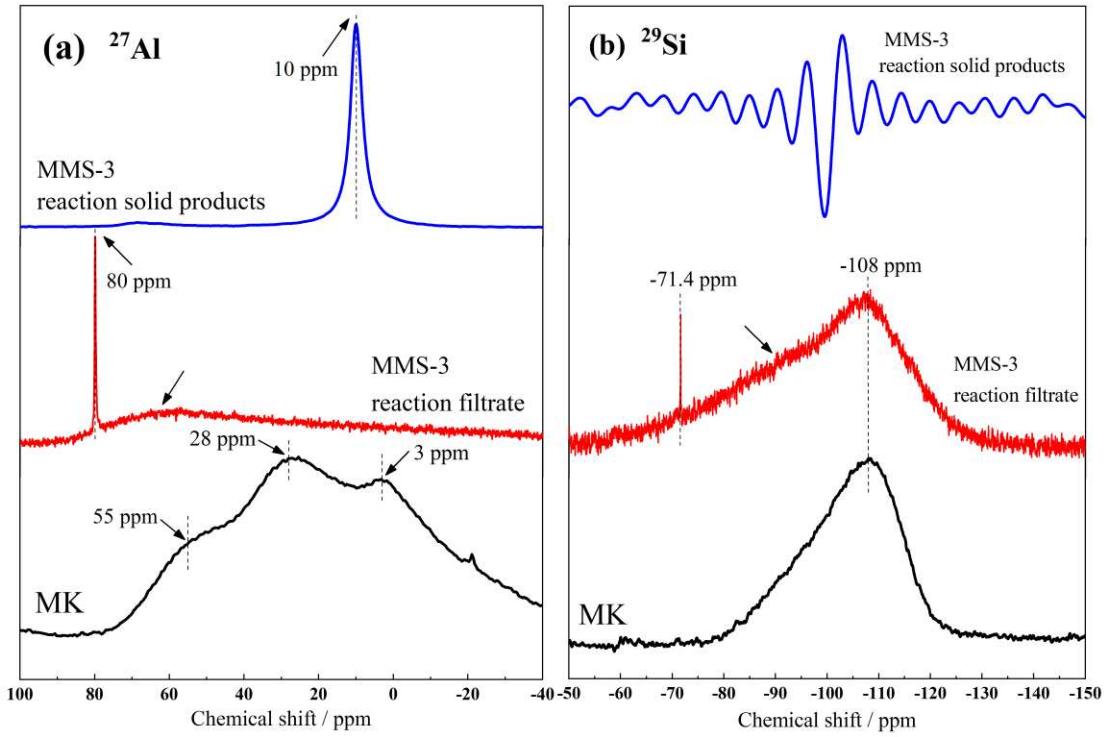

369

370 Fig. 10. (a) ^{27}Al and (b) ^{29}Si MAS-NMR spectra for the raw material MK, reaction
371 filtrate and solid products of sample MMS-3 (6:2:1-60L-6M-80℃).

372 Fig. 10 shows that the signals of ^{27}Al from raw MK include three Al environments with
373 chemical shifts peaked at 55 ppm, 28 ppm and 3 ppm, which can be designated as Al^{IV},

374 Al^{V} and Al^{VI} respectively (Mo et al., 2018). The ^{29}Si signal of MK is mainly a wide
375 resonance centered at -108 ppm, which can be assigned to a series of Al-O-Si bond
376 angles (Singh et al., 2005). After alkali leaching, the ^{27}Al signal in the filtrate is
377 concentrated at 80 ppm, showing that the main form of Al in the solution is $[Al(OH)_4]^-$
378 (Granizo et al., 2014; Weng and Sagoe-Crentsil, 2007). In addition, a broad band at 50-
379 80 ppm is also present, which may be due to the formation of a small amount of
380 aluminosilicate oligomers (Benavent et al., 2016). The ^{29}Si signal in the filtrate is
381 generally similar to that in the raw MK, while a strong and sharp signal appears at 71.4
382 ppm, which can be attributed to $[SiO(OH)_3]^-$ and $[SiO_2(OH)_2]^{2-}$ monomers (Granizo et
383 al., 2014). The original peak at -108 ppm is reduced along with the increased intensity
384 of the broad band between -70 and -108 ppm, indicating more Al coordination with Si
385 (Q^4(mAl)). The ^{29}Si signal in solid product is very weak, indicating negligible Si
386 content, which is consistent with XRD and FTIR results. For ^{27}Al, a strong and sharp
387 signal at 10 ppm is observed in the solid product. Combined with XRD, this indicates
388 that Al in the synthesized LDH is six-fold coordinated, octahedral and very stable
389 (Vyalikh et al., 2009). On the other hand, the ^{27}Al signal of sodium aluminosilicate gel
390 and zeolites tends to concentrate at ~60 ppm due to the formation of Q^4(mAl) sites
391 (Granizo et al., 2014; Singh et al., 2005), which confirms the absence of such
392 aluminosilicates in sampleMMS-3.
393 In the process of LDH formation, the coordination number of Al underwent a
394 significant change from 4 to 6 (i.e., tetrahedra to octahedral structure). In the presence
395 of MgO, Mg^{2+} released and coprecipitated with $[Al(OH)_4]^-$ to form LDH but Si

remained in the solution. With the precipitation of LDH, the amount of free $[Al(OH)_4]^-$ ions in the solution was reduced, leading to higher Si/Al ratio over time. (Sagoe-Crentsil and Weng, 2007) found that when the Si/Al ratio was greater than 3, the condensation reaction between $[Al(OH)_4]^-$ and silicate materials became fast, forming aluminum silicate oligomers which condense to form a grid structure. This may explain that LDH was formed first followed by zeolite and sodalite as shown in Fig. 3. Lower temperature reduced the reaction rate, and thereby prolonged the time required for the formation of LDH. As the reaction time increased, it changed the Si/Al ratio in the solution and hence affected the mineral composition of the precipitated product.

5. Conclusion

This study demonstrated for the first time the feasibility of using solid MgO and MK as the Mg and Al sources respectively to produce Mg-Al LDH. The facile, one-pot synthesis was carried out under the alkaline condition in a water bath at elevated temperatures (<100℃). The formation of LDH was influenced by various parameters such as liquid/solid ratio, temperature, and alkali concentration. The alkali concentration was found to be the key influencing factor since a strong alkaline solution was needed to break the stable silicon-oxy-aluminum bond in the MK to release the trivalent Al. Increasing reaction temperature led to faster dissolution of MK, releasing more Al and Si ions to participate in the reactions. It was also proved that the Mg^{2+} released via MgO hydrolysis combined with $[Al(OH)_4]^-$ ions directly to precipitate LDH whereas brucite when precipitated remained stable in a strong alkaline

environment, contributing little to the formation of LDH. Zeolites and sodalite may form depending on the Si/Al ratio of the solution which was governed by the synthesis parameters. These findings would promote the concept of green chemistry and facilitate the use of widely-available, low-cost natural minerals to produce LDH and zeolite-based materials with wide-ranging environmental and engineering applications. The life cycle assessment on the LDH synthesized through this one-pot process will be further performed in our upcoming research.

Acknowledgments

Authors are pleased to acknowledge the financial supports from National Natural Science Foundation of China (51878346), the Priority Academic Program Development of Jiangsu Higher Education Institutions and Henan Xiaowei Enviroment Technology Co.

References

2020. Mineral commodity summaries 2020, in: summaries, M.c. (Ed.), Mineral Commodity Summaries, Reston, VA, p. 204.

Alothman, Z.A., 2012. A Review: Fundamental Aspects of Silicate Mesoporous Materials. Materials 5, 2874-2902.

Ay, A.N., Zümreoglu-Karan, B., Temel, A., Rives, V., 2009. Bioinorganic Magnetic Core−Shell Nanocomposites Carrying Antiarthritic Agents: Intercalation of Ibuprofen and Glucuronic Acid into Mg−Al−Layered Double Hydroxides Supported on Magnesium Ferrite. Inorganic Chemistry 48, 8871-8877.

Benavent, V., Steins, P., Sobrados, I., Sanz, J., Lambertin, D., Frizon, F., Rossignol, S., Poulesquen, A., 2016. Impact of aluminum on the structure of geopolymers from the early stages to consolidated material. Cement and Concrete Research 90, 27-35.

Budhysutanto, W.N., van Agterveld, D., Schomaker, E., Talma, A.G., Kramer, H.J.M., 2010. Stability and transformation kinetics of 3R1 and 3R2 polytypes of Mg–Al layered double hydroxides. Applied Clay Science 48, 208-213.

Bukhtiyarova, M.V., 2019. A review on effect of synthesis conditions on the formation of layered double

hydroxides. Journal of Solid State Chemistry 269, 494-506.
Chubar, N., Gilmour, R., Gerda, V., Mičušík, M., Omastova, M., Heister, K., Man, P., Fraissard, J., Zaitsev, V., 2017. Layered double hydroxides as the next generation inorganic anion exchangers: Synthetic methods versus applicability. Advances in Colloid and Interface Science 245, 62-80.
Daud, M., Hai, A., Banat, F., Wazir, M.B., Habib, M., Bharath, G., Al-Harthi, M.A., 2019. A review on the recent advances, challenges and future aspect of layered double hydroxides (LDH) – Containing hybrids as promising adsorbents for dyes removal. Journal of Molecular Liquids 288, 110989.
Del Hoyo, C., 2007. Layered double hydroxides and human health: An overview. Applied Clay Science 36, 103-121.
Fan, G.L., Li, F., Evans, D.G., Duan, X., 2014. Catalytic applications of layered double hydroxides: recent advances and perspectives. Chem. Soc. Rev. 43, 7040-7066.
Fan, K., Chen, H., Ji, Y.F., Huang, H., Claesson, P.M., Daniel, Q., Philippe, B., Rensmo, H., Li, F.S., Luo, Y., Sun, L.C., 2016. Nickel-vanadium monolayer double hydroxide for efficient electrochemical water oxidation. Nat. Commun. 7, 9.
Ferencz, Z., Kukovecz, Á., Kónya, Z., Sipos, P., Pálinkó, I., 2015. Optimisation of the synthesis parameters of mechanochemically prepared CaAl-layered double hydroxide. Applied Clay Science 112-113, 94-99.
Gao, Y.S., Wu, J.W., Wang, Q., Wilkie, C.A., O'Hare, D., 2014. Flame retardant polymer/layered double hydroxide nanocomposites. J. Mater. Chem. A 2, 10996-11016.
Goh, K.-H., Lim, T.-T., Dong, Z., 2008. Application of layered double hydroxides for removal of oxyanions: A review. Water Research 42, 1343-1368.
Granizo, N., Palomo, A., Fernandez-Jiménez, A., 2014. Effect of temperature and alkaline concentration on metakaolin leaching kinetics. Ceramics International 40, 8975-8985.
Gu, Z., Atherton, J.J., Xu, Z.P., 2015. Hierarchical layered double hydroxide nanocomposites: structure, synthesis and applications. Chem Commun (Camb) 51, 3024-3036.
Gunjakar, J.L., Kim, T.W., Kim, H.N., Kim, I.Y., Hwang, S.J., 2011. Mesoporous Layer-by-Layer Ordered Nanohybrids of Layered Double Hydroxide and Layered Metal Oxide: Highly Active Visible Light Photocatalysts with Improved Chemical Stability. Journal of the American Chemical Society 133, 14998-15007.
Guzmán-Vargas, A., Santos-Gutiérrez, T., Lima, E., Flores-Moreno, J.L., Oliver-Tolentino, M.A., Martínez-Ortiz, M.d.J., 2015. Efficient KF loaded on MgCaAl hydrotalcite-like compounds in the transesterification of Jatropha curcas oil. Journal of Alloys and Compounds 643, S159-S164.
Halajnia, A., Oustan, S., Najafi, N., Khataee, A.R., Lakzian, A., 2012. The adsorption characteristics of nitrate on Mg–Fe and Mg–Al layered double hydroxides in a simulated soil solution. Applied Clay Science 70, 28-36.
Halajnia, A., Oustan, S., Najafi, N., Khataee, A.R., Lakzian, A., 2013. Adsorption–desorption characteristics of nitrate, phosphate and sulfate on Mg–Al layered double hydroxide. Applied Clay Science 80-81, 305-312.
Hosni, K., Srasra, E., 2009. Simplified synthesis of layered double hydroxide using a natural source of magnesium. Applied Clay Science 43, 415-419.
Hosni, K., Srasra, E., 2010. Evaluation of phosphate removal from water by calcined-LDH synthesized from the dolomite. Colloid Journal 72, 423-431.
Hu, P., Zhang, Y.H., Lv, F.Z., Tong, W.S., Xin, H., Meng, Z.L., Wang, X.K., Chu, P.K., 2017. Preparation of layered double hydroxides using boron mud and red mud industrial wastes and adsorption mechanism

489 to phosphate. Water Environ. J. 31, 145-157.
490 Huang, P.-P., Cao, C.-Y., Wei, F., Sun, Y.-B., Song, W.-G., 2015. MgAl layered double hydroxides with
491 chloride and carbonate ions as interlayer anions for removal of arsenic and fluoride ions in water. RSC
492 Advances 5, 10412-10417.
493 Jitianu, M., Gunness, D.C., Aboagye, D.E., Zaharescu, M., Jitianu, A., 2013. Nanosized Ni–Al layered
494 double hydroxides—Structural characterization. Materials Research Bulletin 48, 1864-1873.
495 Kameda, T., Yoshioka, T., Yabuuchi, F., Uchida, M., Okuwaki, A., 2007. Preparation of a hydrotalcite-
496 like compound using calcined dolomite and polyaluminum chloride. Journal of Materials Science 42,
497 2194-2197.
498 Ladewig, K., Xu, Z.P., Lu, G.Q., 2009. Layered double hydroxide nanoparticles in gene and drug delivery.
499 Expert Opin. Drug Deliv. 6, 907-922.
500 Lei, C., Zhu, X., Zhu, B., Jiang, C., Le, Y., Yu, J., 2017. Superb adsorption capacity of hierarchical
501 calcined Ni/Mg/Al layered double hydroxides for Congo red and Cr(VI) ions. Journal of Hazardous
502 Materials 321, 801-811.
503 Leofanti, G., Padovan, M., Tozzola, G., Venturelli, B., 1998. Surface area and pore texture of catalysts.
504 Catalysis Today 41, 207-219.
505 Liang, X., Zang, Y., Xu, Y., Tan, X., Hou, W., Wang, L., Sun, Y., 2013. Sorption of metal cations on
506 layered double hydroxides. Colloids and Surfaces A: Physicochemical and Engineering Aspects 433,
507 122-131.
508 Liu, Y., Yan, C., Qiu, X., Li, D., Wang, H., Alshameri, A., 2016. Preparation of faujasite block from fly
509 ash-based geopolymer via in-situ hydrothermal method. Journal of the Taiwan Institute of Chemical
510 Engineers 59, 433-439.
511 Lopez, T., Bosch, P., Ramos, E., Gomez, R., Novaro, O., Acosta, D., Figueras, F., 1996. Synthesis and
512 characterization of sol-gel hydrotalcites. Structure and texture. Langmuir 12, 189-192.
513 Mao, N., Zhou, C.H., Keeling, J., Fiore, S., Zhang, H., Chen, L., Jin, G.C., Zhu, T.T., Tong, D.S., Yu,
514 W.H., 2018. Tracked changes of dolomite into Ca-Mg-Al layered double hydroxide. Applied Clay
515 Science 159, 25-36.
516 Mao, N., Zhou, C.H., Tong, D.S., Yu, W.H., Cynthia Lin, C.X., 2017. Exfoliation of layered double
517 hydroxide solids into functional nanosheets. Applied Clay Science 144, 60-78.
518 Mejias, J.A., Berry, A.J., Refson, K., Fraser, D.G., 1999. The kinetics and mechanism of MgO dissolution.
519 Chemical Physics Letters 314, 558-563.
520 Miyata, S., 1975. The Syntheses of Hydrotalcite-Like Compounds and Their Structures and Physico-
521 Chemical Properties—I: the Systems Mg 2+-Al 3+-NO 3−, Mg 2+-Al 3+-Cl−, Mg 2+-Al 3+-ClO 4−, Ni
522 2+-Al 3+-Cl− and Zn 2+-Al 3+-Cl−. Clays and Clay Minerals 23, 369-375.
523 Mo, L., Deng, M., Tang, M., 2010. Effects of calcination condition on expansion property of MgO-type
524 expansive agent used in cement-based materials. Cement and Concrete Research 40, 437-446.
525 Mo, L., Fang, J., Huang, B., Wang, A., Deng, M., 2019. Combined effects of biochar and MgO expansive
526 additive on the autogenous shrinkage, internal relative humidity and compressive strength of cement
527 pastes. Construction and Building Materials 229.
528 Mo, L., Lv, L., Deng, M., Qian, J., 2018. Influence of fly ash and metakaolin on the microstructure and
529 compressive strength of magnesium potassium phosphate cement paste. Cement and Concrete Research
530 111, 116-129.
531 Newman, S.P., Jones, W., O'Connor, P., Stamires, D.N.J.J.o.M.C., 2002. Synthesis of the 3R 2 polytype
532 of a hydrotalcite-like mineral. Journal of Materials Chemistry 12, 153-155.

Nyambo, C., Songtipya, P., Manias, E., Jimenez-Gasco, M.M., Wilkie, C.A., 2008. Effect of MgAl-layered double hydroxide exchanged with linear alkyl carboxylates on fire-retardancy of PMMA and PS. Journal of Materials Chemistry 18, 4827-4838.

Ogawa, M., Kaiho, H., 2002. Homogeneous Precipitation of Uniform Hydrotalcite Particles. Langmuir 18, 4240-4242.

Olanrewaju, J., Newalkar, B.L., Mancino, C., Komarneni, S., 2000. Simplified synthesis of nitrate form of layered double hydroxide. Materials Letters 45, 307-310.

Paikaray, S., Gomez, M.A., Hendry, M.J., Essilfie-Dughan, J., 2014. Formation mechanism of layered double hydroxides in Mg2+-, Al3+-, and Fe3+-rich aqueous media: Implications for neutralization in acid leach ore milling. Applied Clay Science 101, 579-590.

Panda, H.S., Srivastava, R., Bahadur, D., 2011. Synthesis and in situ mechanism of nuclei growth of layered double hydroxides. Bulletin of Materials Science 34, 1599-1604.

Poon, C.S., Lam, L., Kou, S.C., Wong, Y.L., Wong, R., 2001. Rate of pozzolanic reaction of metakaolin in high-performance cement pastes. Cement and Concrete Research 31, 1301-1306.

Qu, J., Zhang, Q., Li, X., He, X., Song, S., 2016. Mechanochemical approaches to synthesize layered double hydroxides: a review. Applied Clay Science 119, 185-192.

Ram Reddy, M.K., Xu, Z.P., Lu, G.Q., Diniz da Costa, J.C., 2006. Layered Double Hydroxides for CO2 Capture: Structure Evolution and Regeneration. Industrial & Engineering Chemistry Research 45, 7504-7509.

Rashad, A.M., 2013. Metakaolin as cementitious material: History, scours, production and composition – A comprehensive overview. Construction and Building Materials 41, 303-318.

Rezvani, Z., Khodam, F., Mokhtari, A., Nejati, K., 2014. Amine-Assisted Syntheses of Carbonate-Free and Highly Crystalline Nitrate-Containing Zn-Al Layered Double Hydroxides. Zeitschrift für anorganische und allgemeine Chemie 640, 2203-2207.

Rożek, P., Król, M., Mozgawa, W., 2018. Spectroscopic studies of fly ash-based geopolymers. Spectrochimica Acta Part A: Molecular and Biomolecular Spectroscopy 198, 283-289.

Rożek, P., Król, M., Mozgawa, W., 2019. Geopolymer-zeolite composites: A review. Journal of Cleaner Production 230, 557-579.

Sagoe-Crentsil, K., Weng, L., 2007. Dissolution processes, hydrolysis and condensation reactions during geopolymer synthesis: Part II. High Si/Al ratio systems. Journal of Materials Science 42, 3007-3014.

Sajid, M., Basheer, C., 2016. Layered double hydroxides: Emerging sorbent materials for analytical extractions. TrAC Trends in Analytical Chemistry 75, 174-182.

Salomão, R., Milena, L.M., Wakamatsu, M.H., Pandolfelli, V.C., 2011. Hydrotalcite synthesis via co-precipitation reactions using MgO and Al(OH)3 precursors. Ceramics International 37, 3063-3070.

Siebecker, M.G., Li, W., Sparks, D.L., 2018. The Important Role of Layered Double Hydroxides in Soil Chemical Processes and Remediation: What We Have Learned Over the Past 20 Years. Advances in Agronomy 147, 1-59.

Singh, P.S., Trigg, M., Burgar, I., Bastow, T., 2005. Geopolymer formation processes at room temperature studied by Si-29 and Al-27 MAS-NMR. Mater. Sci. Eng. A-Struct. Mater. Prop. Microstruct. Process. 396, 392-402.

Stanimirova, T., Hibino, T., Balek, V., 2006. Thermal behavior of Mg-Al-CO3 layered double hydroxide characterized by emanation thermal analysis. Journal of Thermal Analysis and Calorimetry 84, 473-478.

Theiss, F.L., Ayoko, G.A., Frost, R.L., 2016. Synthesis of layered double hydroxides containing Mg2+, Zn2+, Ca2+ and Al3+ layer cations by co-precipitation methods—A review. Applied Surface Science

383, 200-213.
Tongamp, W., Zhang, Q., Saito, F., 2007. Preparation of meixnerite (Mg-Al-OH) type layered double hydroxide by a mechanochemical route. Journal of Materials Science 42, 9210-9215.
Tran, H.N., Lin, C.-C., Woo, S.H., Chao, H.-P., 2018. Efficient removal of copper and lead by Mg/Al layered double hydroxides intercalated with organic acid anions: Adsorption kinetics, isotherms, and thermodynamics. Applied Clay Science 154, 17-27.
Vyalikh, A., Massiot, D., Scheler, U., 2009. Structural characterisation of aluminium layered double hydroxides by 27Al solid-state NMR. Solid State Nuclear Magnetic Resonance 36, 19-23.
Wang, W., Zhang, N., Ye, Z., Hong, Z., Zhi, M., 2019. Synthesis of 3D hierarchical porous Ni-Co layered double hydroxide/N-doped reduced graphene oxide composites for supercapacitor electrodes. Inorganic Chemistry Frontiers 6, 407-416.
Wang, W., Zhou, J., Achari, G., Yu, J., Cai, W., 2014. Cr(VI) removal from aqueous solutions by hydrothermal synthetic layered double hydroxides: Adsorption performance, coexisting anions and regeneration studies. Colloids and Surfaces A: Physicochemical and Engineering Aspects 457, 33-40.
Wang, X., Bai, Z., Zhao, D., Chai, Y., Guo, M., Zhang, J., 2013. New synthetic route to Mg-Al-CO3 layered double hydroxide using magnesite. Materials Research Bulletin 48, 1228-1232.
Weng, L., Sagoe-Crentsil, K., 2007. Dissolution processes, hydrolysis and condensation reactions during geopolymer synthesis: Part I - Low Si/Al ratio systems. Journal of Materials Science 42, 2997-3006.
Xu, Z.P., Lu, G.Q., 2005. Hydrothermal Synthesis of Layered Double Hydroxides (LDHs) from Mixed MgO and Al2O3: LDH Formation Mechanism. Chemistry of Materials 17, 1055-1062.
Yang, Y.M., Zhao, X.F., Zhu, Y., Zhang, F.Z., 2012. Transformation Mechanism of Magnesium and Aluminum Precursor Solution into Crystallites of Layered Double Hydroxide. Chemistry of Materials 24, 81-87.
Yi, Y., Liska, M., Jin, F., Al-Tabbaa, A., 2016. Mechanism of reactive magnesia – ground granulated blastfurnace slag (GGBS) soil stabilization. Canadian Geotechnical Journal 53, 773-782.
Zeng, H.-Y., Deng, X., Wang, Y.-J., Liao, K.-B., 2009. Preparation of Mg-Al hydrotalcite by urea method and its catalytic activity for transesterification. AIChE Journal 55, 1229-1235.
Zhang, L., Zhu, J., Jiang, X., Evans, D.G., Li, F., 2006. Influence of nature of precursors on the formation and structure of Cu–Ni–Cr mixed oxides from layered double hydroxides. Journal of Physics and Chemistry of Solids 67, 1678-1686.
Zhang, Z.H., Zhu, H.J., Zhou, C.H., Wang, H., 2016. Geopolymer from kaolin in China: An overview. Applied Clay Science 119, 31-41.
Zhen, T., Zedong, Q., Shuang, L., Xianming, S., 2020. Functionalized layered double hydroxide applied to heavy metal ions absorption: A review. Nanotechnology Reviews 9, 800-819.
Zhou, J., Yang, S., Yu, J., Shu, Z., 2011. Novel hollow microspheres of hierarchical zinc–aluminum layered double hydroxides and their enhanced adsorption capacity for phosphate in water. Journal of Hazardous Materials 192, 1114-1121.
Zhuang, X.Y., Chen, L., Komarneni, S., Zhou, C.H., Tong, D.S., Yang, H.M., Yu, W.H., Wang, H., 2016. Fly ash-based geopolymer: clean production, properties and applications. Journal of Cleaner Production 125, 253-267.
Zubair, M., Daud, M., McKay, G., Shehzad, F., Al-Harthi, M.A., 2017. Recent progress in layered double hydroxides (LDH)-containing hybrids as adsorbents for water remediation. Applied Clay Science 143, 279-292.

Credit Author Statement

Jun Zhu: Methodology, Investigation, Writing - Original Draft

Bin Zeng: Investigation

Liwu Mo: Supervision, Conceptualization, Investigation

Fei Jin: Conceptualization, Writing - Review & Editing

Min Deng: Project administration

Qingtao Zhang: Funding acquisition, Resources